Supplementary Material

Anomalous size dependence of the coercivity of nanopatterned $CrGeTe_3$

Avia Noah[1,2], Nofar Fridman[1,2], Yishay Zur[1,2], Maya Klang[1], Edwin Herrera[3], Jose Antonio Moreno[3], Martin E. Huber[4], Hermann Suderow[3], Hadar Steinberg[1,2], Oded Millo[1,2], and Yonathan Anahory*[1,2]*

[1]The Racah Institute of Physics, The Hebrew University, Jerusalem, 9190401, Israel
[2]Center for Nanoscience and Nanotechnology, Hebrew University of Jerusalem, Jerusalem, 91904, Israel
[3]Laboratorio de Bajas Temperaturas, Unidad Asociada UAM/CSIC, Departamento de Física de la Materia Condensada, Instituto Nicolás Cabrera and Condensed Matter Physics Center (IFIMAC), Universidad Autónoma de Madrid, E-28049 Madrid, Spain
[4]Departments of Physics and Electrical Engineering, University of Colorado Denver, Denver, CO 80217, USA

Email: avia.noah@mail.huji.ac.il, yonathan.anahory@mail.huji.ac.il

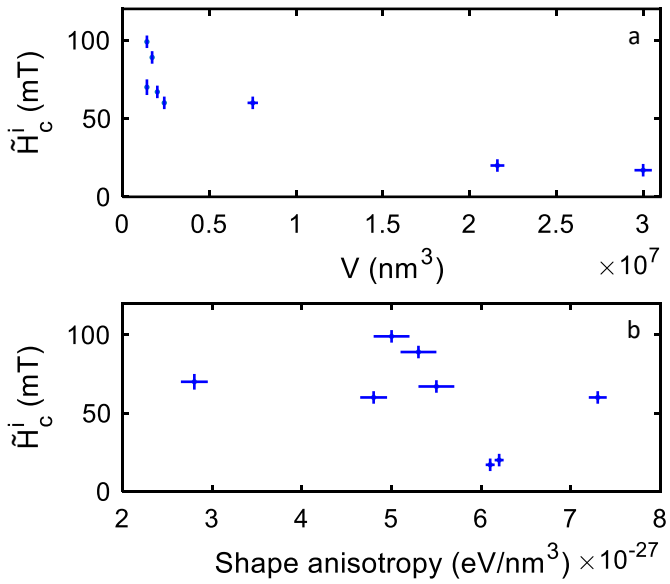

Supplementary Figure 1 - The median island coercive field, $\widetilde{H_c^i}$. (**a**) $\widetilde{H_c^i}$ as a function of island volume V. (**b**) $\widetilde{H_c^i}$ as a function of the island anisotropy**.**

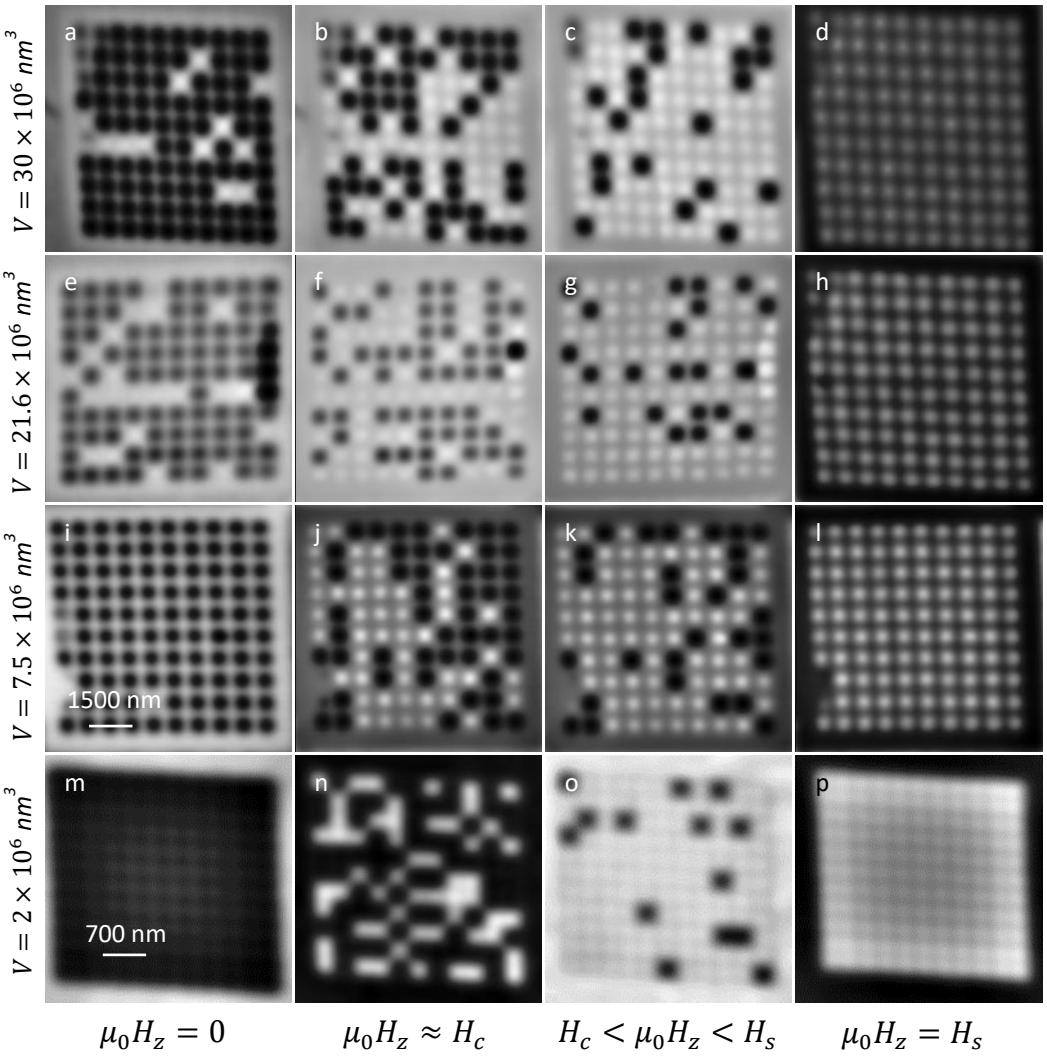

Supplementary Figure 2 - SOT images of nano-patterned island array in $CrGeTe_3$. (**a**-**p**) Sequence of magnetic images $B_z(x, y)$ of different island volumes at distinct values of applied out-of-plane field $\mu_0 H_z$. Imaging parameters: (**a-d**) $V = 30 * 10^6$ nm³, scan area 11 ×11 μm², pixel size 115 nm. $\mu_0 H_z = 0$ **a**, 15 **b**, 30 **c**, 50 mT **d**. (**e-h**) $V = 22 * 10^6$ nm³, scan area 11 ×11 μm², pixel size 115 nm. $\mu_0 H_z = 0$ **e**, 20 **f**, 30 **g**, 50 mT **h**. (**i-l**) $V = 7.5 * 10^6$ nm³, scan area 11×11 μm², pixel size 115 nm. $\mu_0 H_z = 0$ **l**, 60 **j**, 70 **k**, 100 mT **l**. (**m-p**) $V = 2 * 10^6$nm³, scan area 5×5 μm², pixel size 40 nm. $\mu_0 H_z = 0$ **m**, 70 **n**, 90 **o**, 120 mT **p**. The black to white color scale represents lower to higher magnetic fields, respectively.

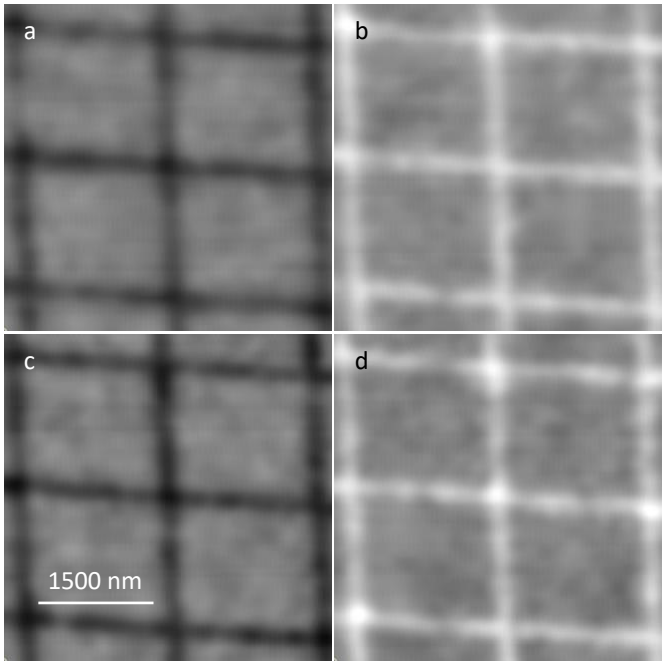

Supplementary Figure 3 - SOT images of magnetic edges due to amorphization in $CrGeTe_3$ at zero field. (**a**-**d**) Sequence of magnetic images $B_z(x, y)$ of amorphized CGT islands after distinct field excursions. (a, c) $H_{exc} < H_s^-$, (b, d) $H_{exc} > H_s^+$. The flake thickness is d = 60 nm. Imaging parameters: $\mu_0 H_z = 0$ mT, area scan 4.2×4.2 μm², pixel size 30 nm. The black to white color scale represents a lower and higher magnetic field, respectively.

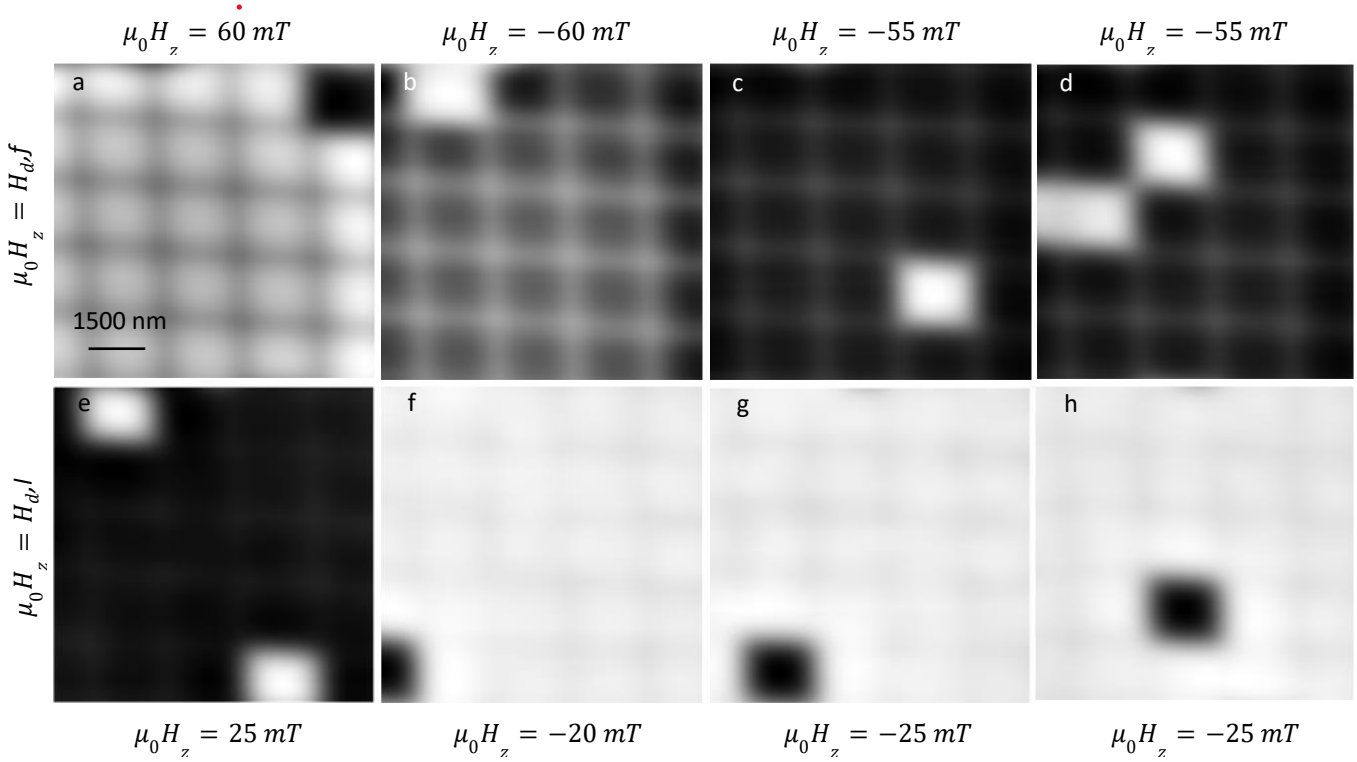

Supplementary Figure 4 – SOT images of the first and last island to demagnetize (**a**-**h**) Magnetic images $B_z(x, y)$ acquired with the SOT that shows the first **a**-**d** and last **e**-**h** to demagnetize in different set of measurements. The field at which the first and last particle demagnetizes is labeled $H_{d,f}$ and $H_{d,l}$, respectively. The black to white color scale represents lower and higher magnetic field, respectively. Each image is 8.5×8.5 μm² and comprise 64×64 pixels.

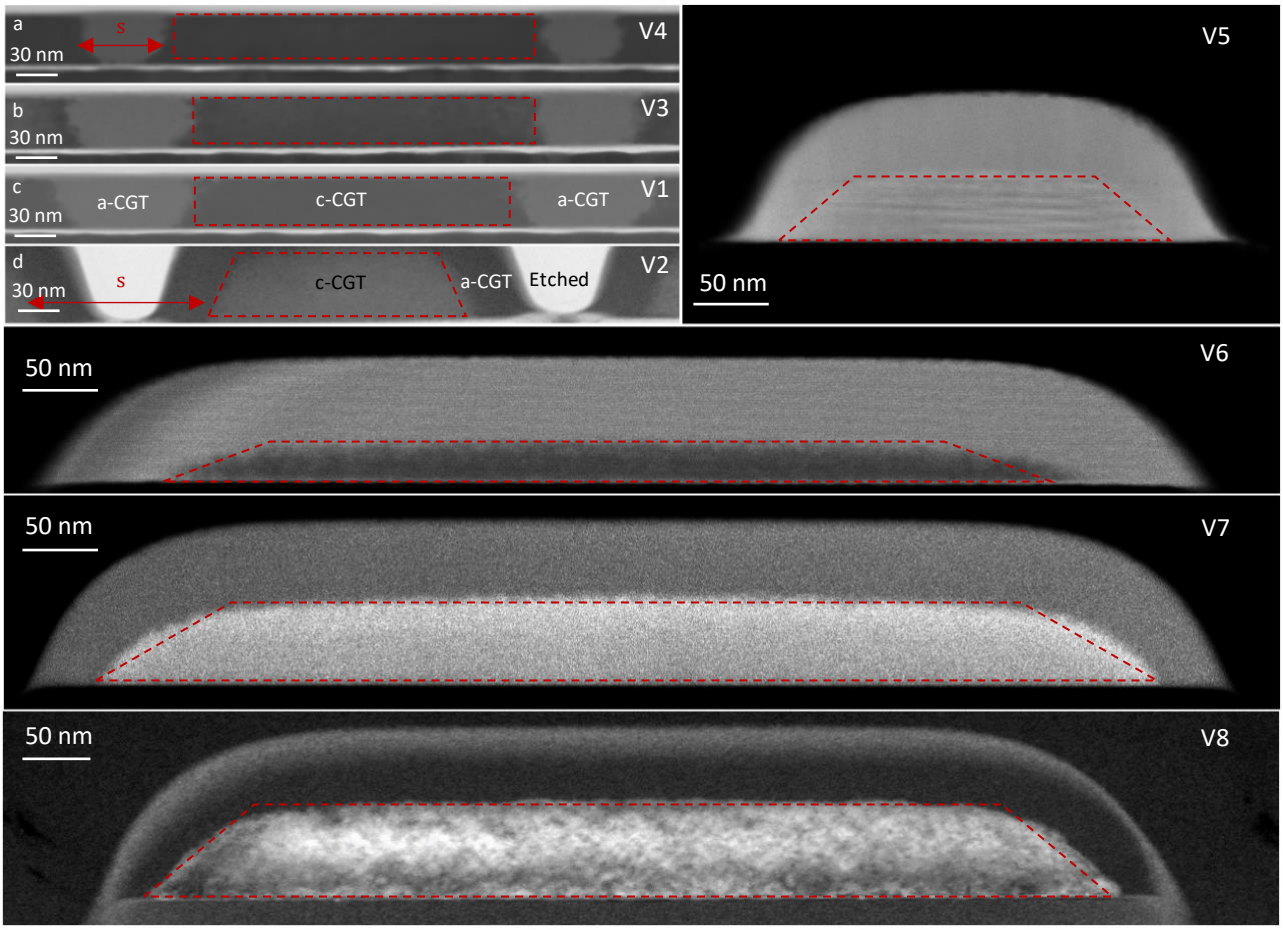

Supplementary Figure 5 - High angle annular dark-HAADF image of each volume the arrays. The area inside the dark red dotted line trapezoid is the region where magnetic crystalline $CrGeTe_3$ is found. Above the crystalline region, an amorphous region is observed for volumes V_2, V_5, V_6, V_7 and V_8.

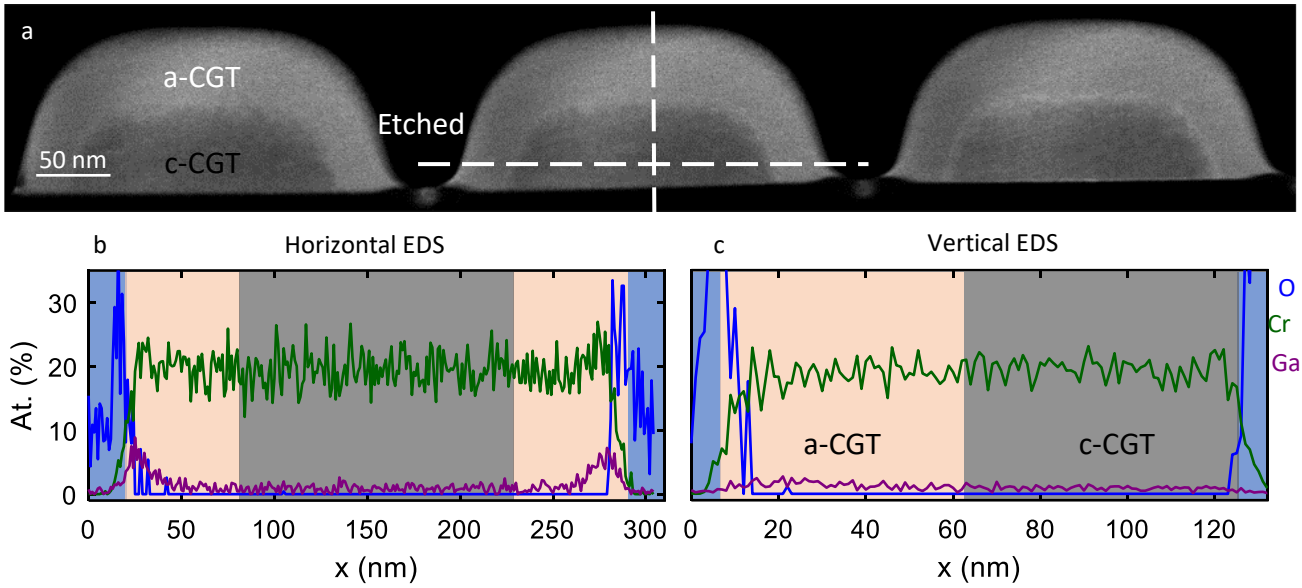

Supplementary Figure 6 – EDS measurements of $CrGeTe_3$ island. (a) High-angle annular dark field (HAADF) image of the V_3array ($150 \times 150 \times 60$ nm³). **(b)** Energy-Dispersive X-ray Spectroscopy (EDS) cross-sections, showing the relative amount of Cr, O, and Ga in a cross section of the island.

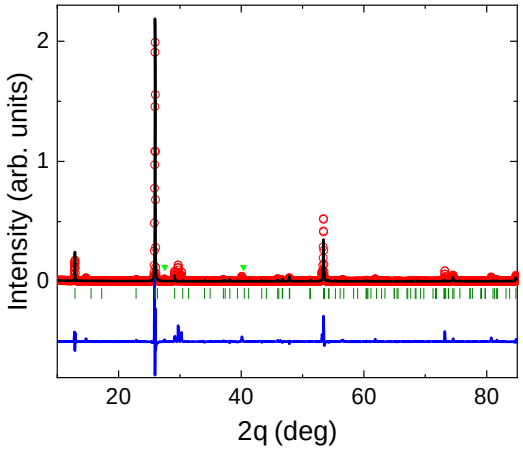

Supplementary Figure 7 - Powder diffraction pattern of $CrGeTe_3$. Red symbols are the experimental points. The black line is the best fit to $CrGeTe_3$ diffraction pattern with refined lattice parameters a = 0.6809 nm, b = 0.6809 nm, c = 2.0444 nm. Residuals are given by the blue line. The vertical green strikes represent the position in 2θ scale of the reflections from the $CrGeTe_3$ (space group R-3h (148)). Green triangles identify the effects of Te flux.

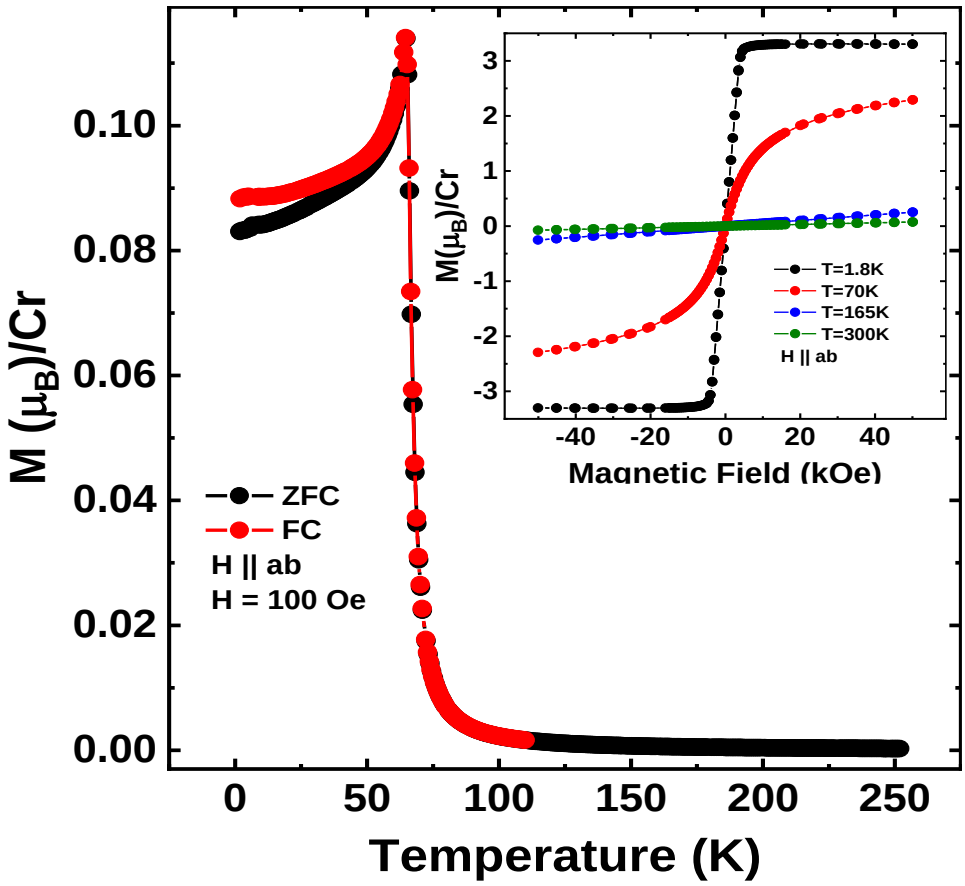

Supplementary Figure 8 – Bulk M(H) measurements. Magnetization as a function of the temperature for ZFC (black symbols) and FC (red symbols) for a magnetic field of 100 Oe applied parallel to the ab-plane. Inset shows Magnetization as a function of the magnetic field for different temperatures.

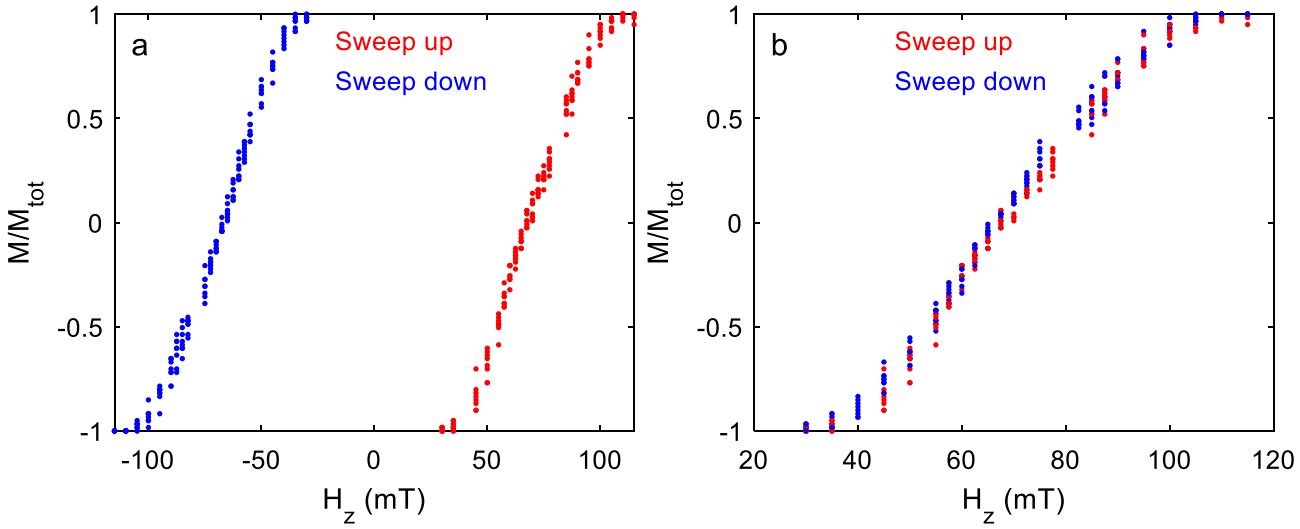

Supplementary Figure 9 - – Measurement reproducibility.. (a) Hysteresis curves drawn from $B_z(x,y)$ images measured for V_4 over 8 complete hysteresis loops. **(b)** Same data as in **a** but showing $M(H)$ for the sweep up (blue dots) and $-M(-H)$ for the sweep down (red dots).

Array name	Number of measured loops	Steps in field (mT) δH_z	Number of Island in the array N	Inter-island Spacing (nm)
V_1	8	2.5	11×11	100
V_2	7	2.5	11×11	80
V_3	3	2.0	9×9	200
V_4	8	2.5	11×11	60
V_5	3	2.5	10×10	200
V_6	5	2.0	10×10	200
V_7	4	2.0	10×10	200
V_8	6	2.0	10×10	200

Supplementary Table 1 – Measurement parameter of the magnetic island array measured and discussed in Figure 2 of the main text. Each array, is named here with the same name as in table 1 and figure 2.

Supplementary Note 1: Sample synthesis and fabrication

Sample synthesis:

Single crystals of $CrGeTe_3$ were grown using slight excess of Te[1,2]. We grew our samples from high-purity Cr (Alfa Aesar 99.999%), Ge (GoodFellow 99.999%) and Te (GoodFellow 99.999%). Cr, Ge and Te were introduced and sealed in quartz ampoules. Then, the ampoules were heated from room temperature to 930 ºC in 12 h, cooled down to 715ºC in 54 h, and finally cooled down to 500 ºC in 54 h; here the samples remain during 99 h. We quenched the crystals down to ambient temperature by immersion in cold water. We obtained layered crystals of 2 mm × 2 mm × 0.5 mm.

Sample fabrication:

CGT samples were fabricated using the dry transfer technique, which was carried out in a glovebox with an argon atmosphere. The CGT flakes were cleaved using the scotch tape method and exfoliated on commercially available Gelfilm from Gelpack. The CGT flakes were transferred onto a SiO_2 substrate. The flakes were exfoliated from the crystals in areas without any Te flux. This was achieved by optically checking that the sample area was free of any inclusions and had large and flat surfaces. The various island shapes were etched or amorphized using a 30 keV Ga^+ focused ion beam (FIB)[3].

Supplementary Note 2: Sample characterization:

Scanning transmission electron microscopy images of $CrGeTe_3$ islands:

Lamellas were prepared and imaged by Helios Nanolab 460F1 Lite focused ion beam (FIB) - Thermo Fisher Scientific. The site-specific thin lamella was extracted from the CGT array using FIB lift-out techniques[4]. Scanning transmission electron microscopy (STEM) and Energy-Dispersive X-ray Spectroscopy (EDS) analyses were conducted using an Aberration Prob-Corrected S/TEM Themis Z G3 (Thermo Fisher Scientific) operated at 300 KV and equipped with a high-angle annular dark field (HAADF) detector from Fischione Instruments and a Super-X EDS detection system (Thermo Fisher Scientific).

To determine the CGT islands' dimensions, we performed cross-section STEM on all islands presented in Figure 2 of the main text. HAADF STEM images are shown in Supplementary Figure 5.

Energy-Dispersive X-ray Spectroscopy of $CrGeTe_3$ island

In Supplementary Figure 6 we present the High-angle annular dark field (HAADF) image of the $150 \times 150 \times 60$ nm^3 island. The image resolves that the crystal structure is damaged due to the FIB etching. Near the etched area, the material is amorphous (bright gray color scale) where the crystalized CGT appears darker. The images reveal the precise thickness of the flake ($\mathrm{d} = 60 \pm 2$ nm) and the edge cross-section $\mathrm{w} = 150 \pm 5$ nm. To understand the stoichiometry of the flakes we perform an energy-dispersive spectroscopy (EDS) measurement. The EDS reveals accumulation of Ga and oxidation peaks near the amorphous edge. The concentration decays abruptly over a length of tens nm. We emphasize that Ga concentration peaks appear only in the amorphous part which we found to be non-magnetic. The Ga in the crystalline area less than 2% according to our EDS measurements. Traces of Silicon were also observed in the EDS measurements which seem to originate from organic residues from the PDMS used during the exfoliation process.

Bulk X-ray diffraction

To characterize the bulk crystals, we made x-ray diffraction on crystals milled down to powder (Supplementary Figure 7). X-ray diffraction experiments were performed using an X-ray Bruker D8 Discover Diffractometer at room temperature. Rietveld analysis was performed on X-ray diffractograms using FullProf suite[5]. After Rietveld refinement, we find $CrGeTe_3$ (space group R-3h (148)), with refined lattice parameters a = 0.6809 nm, b = 0.6809 nm, c = 2.0444 nm, with a small trace of Te (see green triangles in Figure).

Bulk SQUID measurements

Bulk magnetic characterization was performed using a Quantum Design SQUID magnetometer. Supplementary Figure 8 depicts the magnetization of a bulk crystal as a function of temperature $M(T)$. We see a clear transition around the expected Currie temperature $T_c = 65$ K. In the inset of Supplementary Figure 8 we show the magnetization as a function of the applied field $M(H)$. At low temperature we obtain the expected value for the saturation magnetization which is around 3 μ_B/Cr. This value is consistent with the value obtain in previous reports.[6,7]

Supplementary Note 3: Uncertainty estimation

Uncertainty on the island dimensions (w and d)

The uncertainties associated with w and d were estimated from the TEM measurements. In samples with $d = 35$ nm, the islands were created by FIB amorphization. Therefore, the uncertainty in d is only due to oxidation, $\delta d = 2$ nm, and with respect to w it is a fraction of the Ga^+ beam profile $\delta w = 5$ nm. However, other islands were created by FIB etching, resulting in a trapezoid shape, and the islands are covered by amorphized CGT (which is non-magnetic). In this case, the uncertainty is larger because the amorphous area is not well defined in the TEM image. This results in $\delta d = 10$ to 20 nm, and $\delta w = 10$ to 100 nm, depending on the specific case.

To estimate the uncertainty δp in the parameter $p = \frac{w}{V} = \frac{1}{wd}$, we consider the uncertainties associated with each parameter separately and then propagate these uncertainties using the following expression:

$$\delta p = \sqrt{\left(\frac{\partial p}{\partial w} \cdot \delta w\right)^2 + \left(\frac{\partial p}{\partial d} \cdot \delta d\right)^2}$$

Where, δp, δw, and δd are the the uncertainties corresponding to p,w, and d, respectively.

Uncertainty on the median island coercivity $\widetilde{H_c^i}$

The main source of uncertainty is related to the large transition over which the islands reverse their magnetization. If all island were identical and neglecting thermal fluctuations, all island should reverse their magnetization at the same field $\Delta H_z = H_l - H_f$. In all the measured array, the value of ΔH_z was rather nearly constant around 73 mT (see Table 1 in the main text). The other source of uncertainty is the field step separating two measurements, which was around $\delta H_z = 2.5$ mT (see supplementary table 1 for the specific values corresponding to each array.

To estimate the resulting uncertainty on the coercive field δH_c, we consider we sum in quadrature those uncorrelated sources of noise. The uncertainty component generated by ΔH_z is written as $\frac{\mathrm{H}_l - H_f}{2\sqrt{N}}$, where N is the number of island measured in the array (around 100 islands, see Supplementary Table 1 for exact values). In addition given that we consider difference from the mean value we also divide this number by 2. The result is written as follows:

$$\delta H_c = \sqrt{\left(\frac{\mathrm{H}_l - H_f}{2\sqrt{N}}\right)^2 + (\delta H_z)^2} \approx 4 \text{ mT}$$

Reproducibility of the coercivity measurement.

To measure the reproducibility in probing the island median coercive field $\widetilde{H_c^i}$, we measure the array's magnetization $M(H_z)/M_{tot}$ for 8 complete hysteresis loops. The results are presented in Supplementary Figure 9a. We calculate the array's coercive field from the data for each of the 16 occurrences. The obtained standard deviation on the value of H_c is 0.7 mT which is smaller than our uncertainty which is dominated by the width of the transition $\Delta H_z/\sqrt{N} = 8$ mT and the steps size in field $\delta H_z = 2.5$ mT. This suggests that the width of the transition ΔH_z is likely dominated by variability in the island property rather than thermal fluctuations. Further investigation could confirm this finding.

Symmetrization of the $M(H_z)$ curves

We also compare the coercivity measured at $H_z > 0$ and $H_z < 0$ by plotting the $M(H_z)$ for the sweep up with $-M(-H_z)$ for the sweep down (Supplementary Figure 9b). The data overlaps very nicely over the 8 complete hysteresis loops. To further quantify that point, we calculate the array's coercive field for both data sets. We obtain 66.8 ± 0.4 mT and 67.8 ± 0.7 mT for the sweep down and sweep up data, respectively. This justify the symmetrization of our curves in Figure 2a.

Supplementary Note 4: Scanning SQUID-On-Tip microscopy

The SOT was fabricated using self-aligned three-step thermal deposition of Pb at cryogenic temperatures, as described previously[8,9]. The measurements were performed using tips with effective SQUID loop diameters ranging from 145 to 175 nm. All measurements were performed at 4.2 K in a low pressure He of 1 to 10 mbar. The quantification of the measured magnetic field was performed as described previously[8,9].

Reference:

1. Canfield, P. C. Solution Growth of Intermetallic Single Crystals: A Beginner's Guide. in 93–111 (2009). doi:10.1142/9789814261647_0002.
2. Canfield, P. C. & Fisk, Z. Growth of single crystals from metallic fluxes. *Philosophical Magazine B* **65**, 1117–1123 (1992).
3. Noah, A. *et al.* Nano-Patterned Magnetic Edges in CrGeTe3 for Quasi 1-D Spintronic Devices. *ACS Appl Nano Mater* **6**, 8627–8634 (2023).
4. Sezen, M. Focused Ion Beams (FIB) — Novel Methodologies and Recent Applications for Multidisciplinary Sciences. in *Modern Electron Microscopy in Physical and Life Sciences* (InTech, 2016). doi:10.5772/61634.
5. Rodríguez-Carvajal, J. Recent advances in magnetic structure determination by neutron powder diffraction. *Physica B Condens Matter* **192**, 55–69 (1993).
6. Carteaux, V., Brunet, D., Ouvrard, G. & Andre, G. Crystallographic, magnetic and electronic structures of a new layered ferromagnetic compound Cr2Ge2Te6. *Journal of Physics: Condensed Matter* **7**, 69–87 (1995).
7. Ji, H. *et al.* A ferromagnetic insulating substrate for the epitaxial growth of topological insulators. *J Appl Phys* **114**, (2013).
8. Vasyukov, D. *et al.* A scanning superconducting quantum interference device with single electron spin sensitivity. *Nat Nanotechnol* **8**, 639–644 (2013).
9. Anahory, Y. *et al.* SQUID-on-tip with single-electron spin sensitivity for high-field and ultra-low temperature nanomagnetic imaging. *Nanoscale* **12**, 3174–3182 (2020).